Analysis of ball movement for research of grinding mechanism of a stirred ball mill with 3D discrete element method

Seongsoo Kim and Woo Sik Choi*,†

Dept. of Precision & Mechanical Engineering and Eco-Friendly Heat & Cooling Energy Mechanical Research Team, BK21,
Gyeongsang National University, 445 Inpyeong-dong, Tongyoung, Gyeongnam 650-160, Korea
*Dept. of Pharmaceutical Manufacturing, Pusan National University, Busan 609-735, Korea

Abstract−A simulation of the three-dimensional motion of grinding media in the stirred media mill for the research of grinding mechanism has been carried out by 3-dimensional discrete element method (DEM). The movement of ball assemblies was graphically displayed with some snapshots from start of the milling to 0.20 s. From these simulation results, the grinding zone in the mill was confirmed to be distributed into two regions, which is near the stirrer and the side wall of mill around the stirrer. The power changing the rotation speed of stirrer was examined based on the micro interactive forces at all the contact points between ball-to-ball and between ball-to-stirrer. DEM is a very powerful tool for the microanalysis of movement of balls, which could not have been solved by a conventional experimental method.

Key words: DEM, Computer Simulation, Ball Movement, Stirred Ball Mill, Power, Grinding Mechanism

INTRODUCTION

The size reduction and mechano-chemical grinding in a grinding media type of mill are influenced by impact, compression, shear, and friction at all the contact points of balls in the mill. Therefore, understanding the behavior of ball movement in the mill is very important to identify the grinding mechanism and to produce ultra-fine particles for developing new materials.

Stirred grinding media mill has been used as a type of an ultra-fine grinding mill in many industries such as minerals, ceramic materials, chemical products and other materials due to its high energy efficiency, fine and ultra-fine grinding ability, and reduced contamination [1-3]. The computer simulation technique for studying the flow of granular assemblies or powders is useful especially for obtaining detailed results from the task in that direct experimentation is difficult. DEM is a scheme to simulate any problem dealing with the behavior of a discontinuous particle system by Cundall [4], who first used this type of model to study granular assemblies. Since then, these models have become widely applied to the simulation of a discontinuous particle system [5]. Many kinds of simulations for the ball mill have been studied: the 3-dimensional behaviors of ball movement in a tumbling mill [6,7], the power of a tumbling mill [8,9], and the power of a centrifugal mill [10]. However, up to now, there has been little simulation research for stirred grinding media mill. In the stirred ball mill, there are some stirrers and the calculation of its consumed powder becomes more complicated to compare with the simpler kinetics of conventional tumbling ball mill [11,12].

The objective of this paper is to simulate the motion of grinding media balls in stirred grinding media mill and to examine the consumed power based on the micro interactive forces at all the contact points between balls and between ball and stirrer.

SIMULATION ON BALL MOTION IN THE STIRRED MILL

The ball mills of grinding media types, for example, tumbling ball mill, planetary ball mill and stirred grinding media mill are very useful grinding machines used in many fields [13,14]. Furthermore, these mills have been used for activating the mechanical effects as well as the size reduction of materials. The motion of balls in the mill causes impact, compressive and shear forces on the materials during grinding process.

1. Numerical Simulation Procedures
1-1. Ball Movement

The movement calculation of spherical balls is fundamentally performed to mutually apply to the second law of Newton's motion law and the force-displacement law at contact points between balls or ball and wall of pot mill or ball and stirrer. The Voigt model of interactive force between two balls as shown in Fig. 1 is used to simulate the ball movement, in which an elastic spring and a viscous dashpot between balls should be introduced to estimate the forces
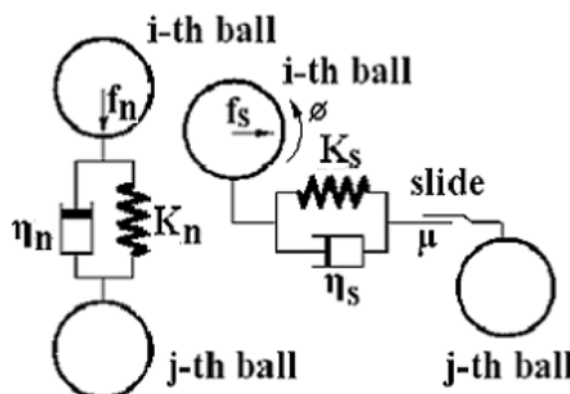

Fig. 1. Voigt model of interactive forces between two balls.

†To whom correspondence should be addressed.
E-mail: wschoi@pusan.ac.kr

produced by the contact of other balls acting on a certain ball. In the shear direction, a friction slider can be also introduced to estimate slip at the contact point.

The motion equation of a ball can be expressed in Eq. (1) for a translation motion and Eq. (2) for revolution motion by considering the interaction forces generated at the contact point when two balls of mass m collide with each other [15].

$$m\frac{d^2u}{dt^2} + \eta\frac{du}{dt} + Ku = 0 \tag{1}$$

$$I\frac{d^2\phi}{dt^2} + \eta r^2\frac{d\phi}{dt} + Kr^2\phi = 0 \tag{2}$$

where m denotes mass, u translation displacement, ϕ revolution displacement, K elasticity modulus, η viscosity coefficient, and I the inertia moment.

Because a lot of ball contacts with one certain ball for a series of other balls, the above Eqs. (1) and (2) are formed at every contact point. The practical calculation is performed by using the difference approximation equation of time difference Δt as shown in Eq. (3).

$$m[\ddot{u}_i]_t = -\eta[\dot{u}_i]_{t-\Delta t} - K[u_i]_{t-\Delta t} \tag{3}$$

The normal and shear relative displacement increments, Δn and Δs are used with the force-displacement law to calculate increments of the normal and shear forces, ΔF_n and ΔF_s.

$$\Delta F_n = k_n\Delta n, \quad \Delta F_s = k_s\Delta s \tag{4}$$

The normal stiffness k_n is obtained by Hertz's contact theory as follows:

$$k_n = \left(\frac{E}{1-\nu_P^2}\right)\left(\frac{D_p}{4}\right)^{1/2}\delta^{1/2} \tag{5}$$

where E, δ and ν_P are the module of elasticity, the accumulated normal displacement, and Poisson's ratio, respectively. In this calculation, we assume that the relation between the normal stiffness k_n and the shear stiffness k_s is $k_s = (1/5)k_n$.

The damping force increments ΔD_n and ΔD_s by viscous dashpot in the normal and shear directions at a contact point are taken to be proportional to the normal and shear components of the relative velocity increments, and as follows:

$$\Delta D_n = -\eta_n\Delta\dot{n}, \quad \Delta D_s = -\eta_s\Delta\dot{s} \tag{6}$$

The normal and the tangential contact forces and the damping forces at time t are as follows:

$$(F_n)_t = (F)_{t-1} + \Delta F_n, \ (F_s)_t = (F_s)_{t-1} + \Delta F_s \tag{7}$$

$$(D_n)_t = (D)_{t-1} + \Delta D_n, \ (D_s)_t = (D_s)_{t-1} + \Delta D_s \tag{8}$$

To solve the governing equations of DEM, the normal damping coefficient η_n and the shear damping coefficient η_s have to satisfy the following relations, respectively:

$$\eta_n = 2\sqrt{m_{pi}k_n}, \quad \eta_s = 2\sqrt{m_{pi}k_s} \tag{9}$$

where m_{pi} is mass of ith ball.

In the shear direction, the following conditions are also required to describe the slip at the contact point:

when $(F_s)_t > \mu(F_n)_t$,

$$(F_s)_t = \text{sign}[(F_s)_t]\cdot\mu_p(F_n)_t \tag{10}$$

and

$$(D_s)_t = 0 \tag{11}$$

where sign $[(F_s)_t]$ is an arithmetic symbol which denotes the sign of $(F_s)_t$ and μ_p is a friction coefficient.

The summation of these contact force components in each direction gives the resultant force, $\sum_j[(F_{nij})_t+(F_{sij})_t+(D_{nij})_t+(D_{sij})_t]$. The resultant moment acting on ball i is found from $\sum_j[(D_p/2)(F_{sij})_t+(D_p/2)(D_{sij})_t]$, where the summation is taken over all the contact points of ball i. Thus, if ball i is displaced independently from any other ball by the resultant force and moment during Δt, the Lagrangian type equations of the ball motion are described as follows.

$$m_{pi}\frac{d(u_{pi})_t}{dt} = \sum_j[(F_{nij})_t+(F_{sij})_t+(D_{nij})_t+(D_{sij})_t] + m_{pi}g \tag{12}$$

$$I_{pi}\frac{d(w_{pi})_t}{dt} = \sum_j\left[\left(\frac{D_p}{2}\right)_t(F_{sij})_t+\left(\frac{D_p}{2}\right)_t(D_{sij})_t\right] \tag{13}$$

where g, I_{pi} and ω_{pi} are the gravitational acceleration, the inertia moment of ball, and the ball angular velocity in vector, respectively. In this study, the forward difference scheme is used for the time derivative terms of Eqs. (12) and (13).

Fig. 2 and Table 1 show the computational domain and the calculation conditions, respectively [13,16]. The shape of a stirrer is simplified to a plate of 3×27 ball matrix for ease of calculation. The
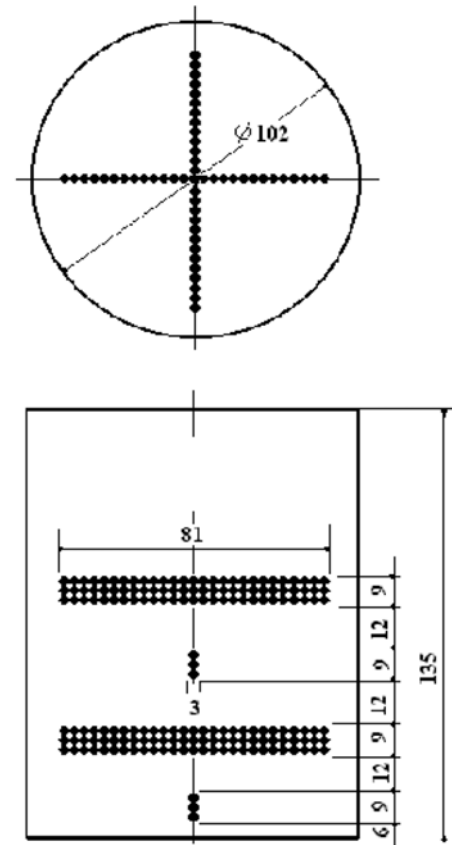

Fig. 2. Computational domain (unit: mm).

Table 1. Calculation conditions for simulation

Dimensions of grinding pot	<Diameter>, D	ϕ 102 mm
Dimensions of grinding pot	<Height>, H	ϕ 135 mm
Dimensions of the stirrer	<Diameter>, D_B	ϕ 81 mm
Dimensions of the stirrer	<Width>, W_B	9 mm
Dimensions of the stirrer	<Thickness>, T_B	3 mm
Dimensions of the stirrer	<Number>, n_B	4*
Rotation speed	N	100-900 rpm
Particle number	n_P	16,736
Particle diameter	D_P	3 mm
Particle density	ρ_p	3.6×10^3 kg/m^3
Particle mass	m_P	5.1×10^{-5} kg
Time step	Δt	2.0×10^{-6} s
Modulus of elasticity <Particle-to-particle>, E_P		2.0×10^9 N/m
Modulus of elasticity <Particle-to-wall>, E_W		2.0×10^9 N/m
Poisson's ratio,	ν	0.25
Damping coefficient <Normal>, η_n		$= 2\sqrt{m_p k_s}$ kg/s
Damping coefficient <Shear>, η_S		$= 2\sqrt{m_p k_s}$ kg/s
Friction coefficient <Particle-to-particle>, μ_P		0.2
Friction coefficient <Particle-to-wall>, μ_w		0.25

*Each stirrer is consisted of in-lined balls of 81.

initial charged position of balls is arranged as shown in Fig. 3 without any contact between balls and stirrers. The material of stirrer and the size of in-lined balls are same as the media balls. The time step in calculation is 2.0×10^{-6} s. The total number of balls to be calculated is 16,736.
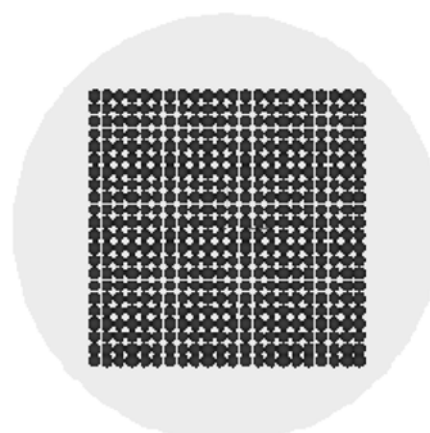
1-2. Power Calculation

To obtain the power of the stirred ball mill, the moment principal was adopted in this work. In Fig. 4, each axial component of the forces acting at contact point c between the i-th ball of blade and the j-th moving contact ball is F_x, F_y, and F_z, which are parallel to the three axes, respectively, where x_c and y_c are the distances from zero point of z axis to a contact point. When the forces are calculated according to the flow chart as shown in Fig. 5, the instantaneous total moment T and power P at the rotation speed n are expressed as Eqs. (14) and (15), respectively,

$$T = \sum_{i=1}^{j\,max} \sum_{tno=1}^{tno\,max} (F_{x,(i,tno)} \cdot y_{c,(i,tno)} + F_{y,(i,tno)} \cdot x_{c,(i,tno)}) \tag{14}$$
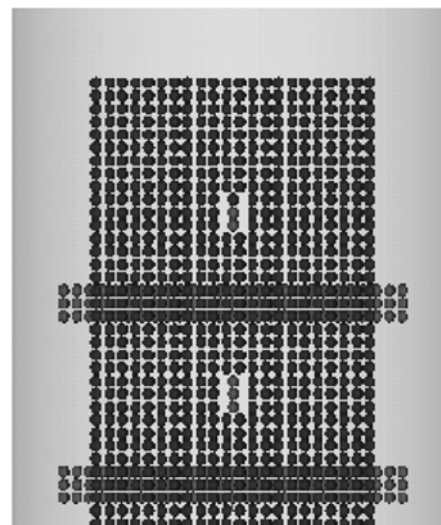
$$P = \frac{2\pi n}{60} \cdot T \tag{15}$$

where j_{max} is the total contact points on blade balls, x_c and y_c the distance from x-axis and y-axis, respectively, and n the rotation speed per minute.
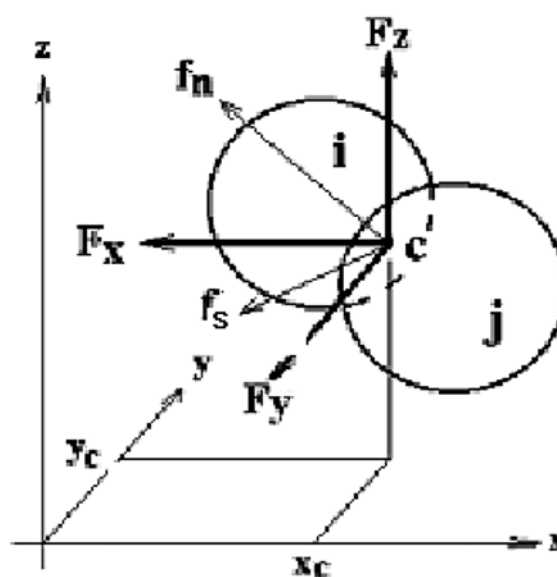
The flow chart of a general calculation is shown in Fig. 5. The values of parameters of materials and the operation conditions of mill are input as shown in Table 1. In addition, a position condition of initial charge of grinding media balls and stirrers is set. When a calculation begins, the balls not to contact each other fall freely while the balls to contact each other or with stirrer move by the rotation of stirrer. This simulation of ball movement is continued till the end of running time.

(a) Top: Plane view

(b) Bottom: Side view

Fig. 3. Initial charge of the balls.

Fig. 4. Forces acting at a contact point between i-th ball of blade and j-th moving ball.
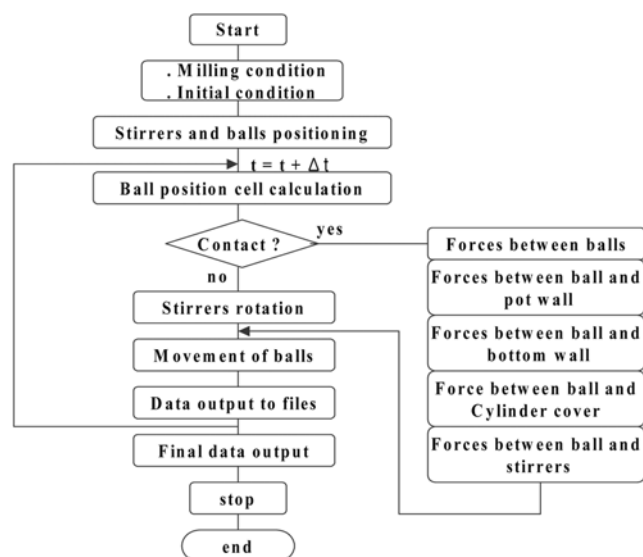
Fig. 5. Flow chart of calculation of power for a stirred mill.

Each ball comes to have the cell information according to the position in the mill. After judgment whether the contact is with ball-to-ball or with ball-to-stirrer or with ball-to-wall of mill or not, the number of contact points and the contact force at each contact point are calculated. Then, the acceleration, velocity, and dislocation of the ball are calculated based on above calculated forces. That is, the ball moves to a new position by the movement displacement during Δt time while the stirrer turns at determined position by rotation during Δt time. For next Δt time, these above calculation procedures for all the balls repeat during predetermined running time.

The programs were coded with MS Fortran 77 for the ball movement and with MS Visual Basic for display of ball movement, re-

spectively. The calculated results at each predetermined time interval are output and display the position of balls in a section of an X-Z axial direction and an X-Y axial direction.

1-3. Experimental

The schematic diagram of experimental equipment used for the comparison with the results of the simulation is shown with the dimension of mill pot in Fig. 6. The mill was a vertical type of stirred ball mill, KMD-1B, made by Korea Material Development Co., Ltd. The size and material of the grinding media ball is 3 mm in diameter with density of 3.6 g/cm^3 and alumina of resistant-attrition, which was made by Nikkado Co. Japan, respectively. The stirrer could be rotated by controller and the power could be measured with self-made measuring devices of power. The moving pattern of grinding media balls in the mill was observed with a home video camera through a transparent cover of the acrylic resin plate.

The materials of pot and ball used in this experiment were the same as those in the case of simulation. The number of balls of Al$_2$O$_3$ used was 16,736. The power was measured with a self-made electronic circuit device. The experimental methods were also same as those in previous papers [2,3].

SIMULATION RESULTS AND CONSIDERATIONS

1. Movement Pattern of Grinding Media Balls

In order to check the applicability of this simulation program, the movement pattern of grinding media balls for the rotation speed of stirrer which varied with from 100 rpm to 700 rpm was observed with a video camera through a transparent cover displaced with acryl resin plate; it was also compared with the photographs and the snapshots of the motion of grinding media balls by simulation (Fig. 7). The good agreement between the experimental flow patterns of balls and the simulation those for the rotation speed of stirrer was confirmed by video photographs and snapshots of balls. That is, the
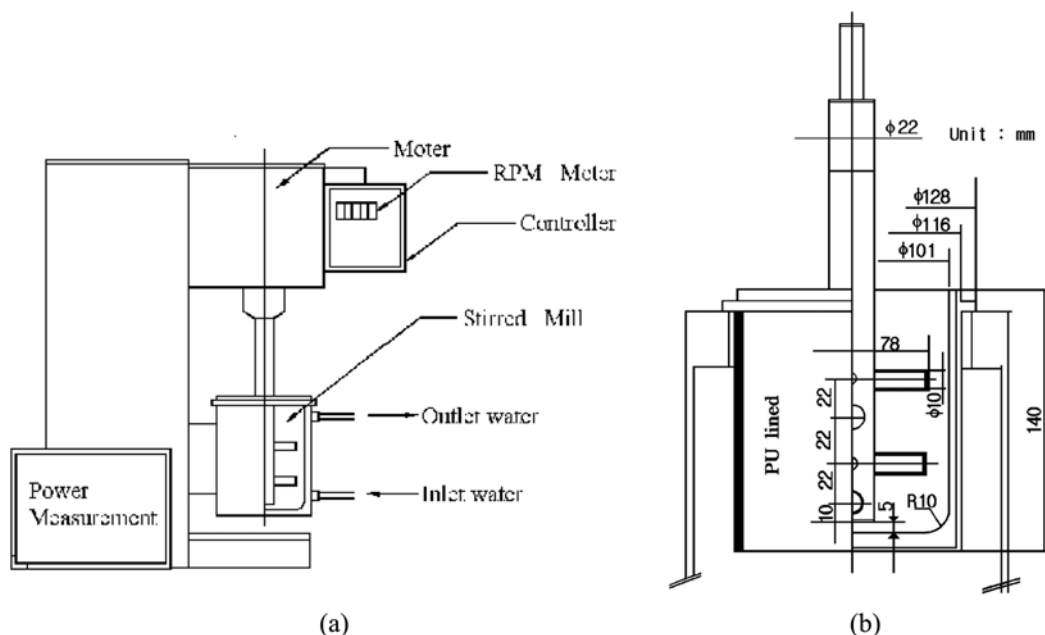

Fig. 6. Schematic diagram of experimental apparatus.
   (a) Stirred ball mill and the measuring system, (b) Dimensions and shape of the grinding mill pot
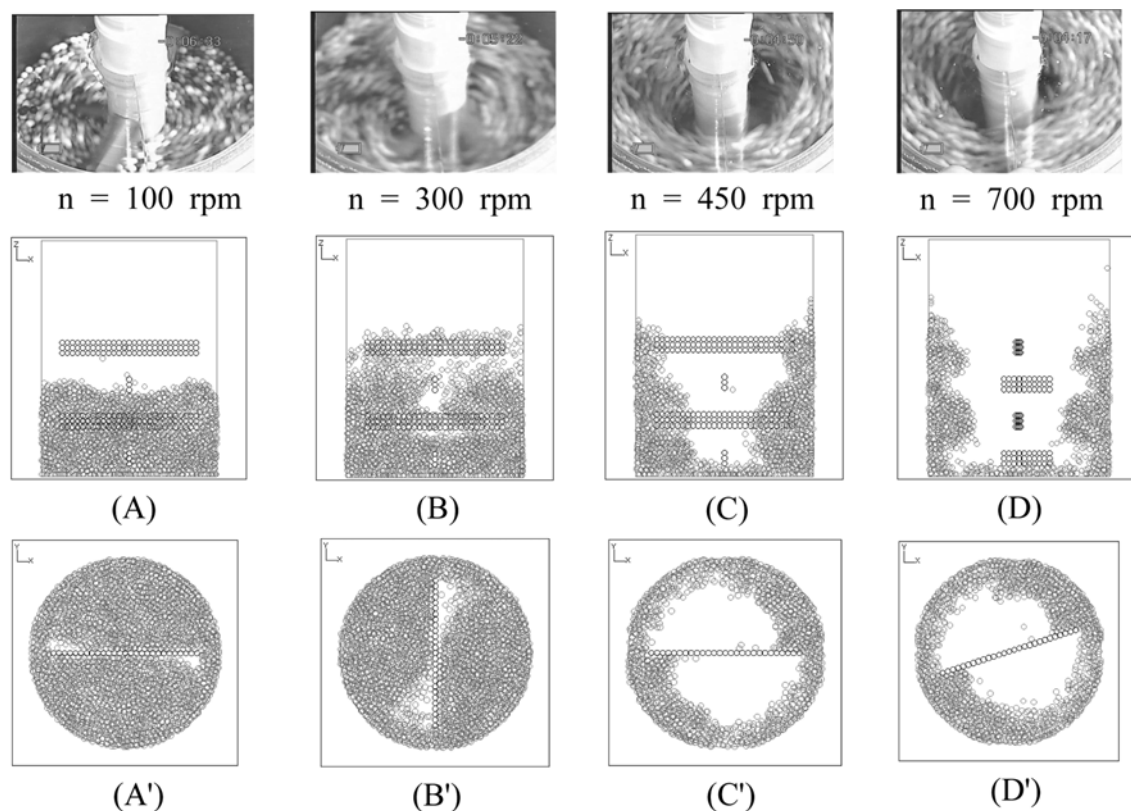
Fig. 7. Snapshots of the motion of grinding media balls by simulation for each rotation speed and photographs of video camera compared with experiments.
Key: Top: Video photographs for each rotation speed, Middle: Snapshots of motion of grinding balls at front view through center, Bottom: Snapshots of motion of grinding balls at overview.

flow pattern of balls shows three types of movement patterns according to the rotation speed of stirrer n by the centrifugal force and gravity force: the first is horizontal flow pattern for n=200 rpm; the second, annular type flow pattern along the wall of pot for n= 450 rpm; and the third, transition state of first and second flow pattern with higher at the wall of pot and with lower and more vacant at center of pot.

Fig. 8 shows snapshots of the motion of grinding media balls by simulation around the stirrers rotating at 300 rpm for 0 to 0.20 s of grinding time. As the stirrers rotate in counterclockwise direction, the ball assemblies are falling down simultaneously and begin to scatter to the wall by the contact with the stirrers.

When the grinding time as shown in Fig. 8(e) passed 0.16 s, all the balls were scattered randomly to the wall of grinding mill pot. Here, it could be assumed that many kinds of forces for the grinding could be generated such as impact, collision, friction, compress, shear and so on. As the grinding time goes on, at Fig. 8(f), ball assemblies are scattered and then stick to the wall. The upper two stirrers are revealed clearly in sight of the upper; the level of the highest ball assemblies is the same as that of the top stirrer.

Fig. 9 shows snapshots of the movement of balls by simulation on the sectional plane including an axis at the rotation speed of 300, 500, and 700 rpm, respectively. As the rotation speed is higher, the balls are concentrated to the pot wall and move upward, and then the middle part of the pot is vacant. At each rotation speed of stirrer, the highest position of balls shows somewhat like the free surface
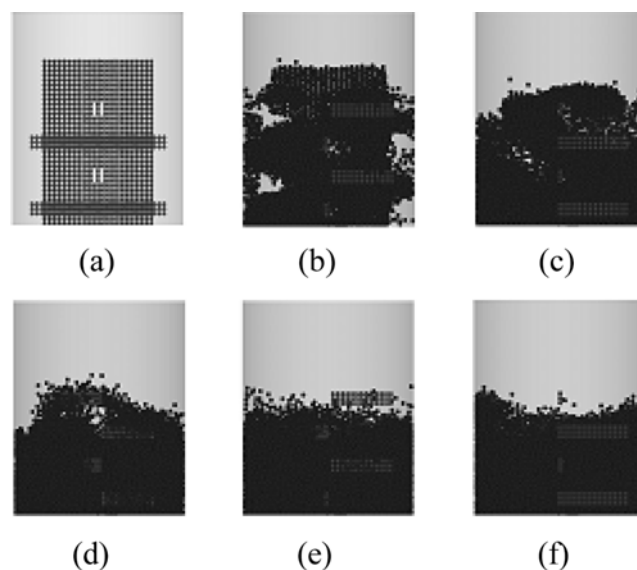

Fig. 8. Snapshots of the motion of grinding media balls around the stirrers rotated in 300 rpm from 0 to 0.20 s.
(a) Initial state, (b) t=0.04 s, (c) t=0.08 s, (d) t=0.12 s, (e) t= 0.16 s, (f) t=0.20 s

of a liquid. That means the motion of balls is governed under the centrifugal force and gravity force. As the rotation speed is higher,
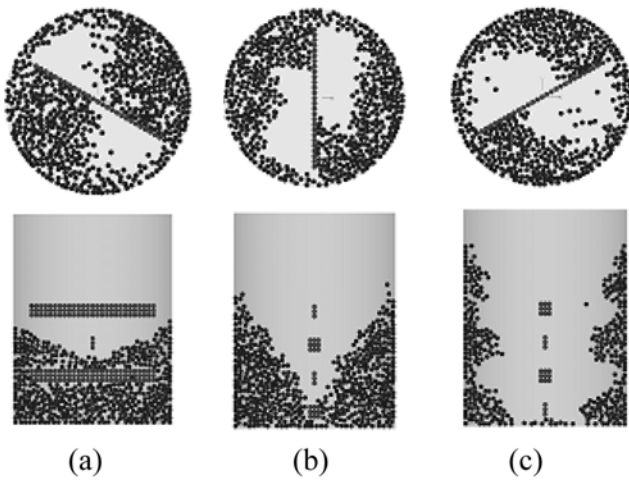
Fig. 9. Snapshots of the motion of grinding media balls at the axis section for rotation speed of stirrer (a) n=300 rpm, (b) n= 500 rpm, and (c) n=700 rpm.
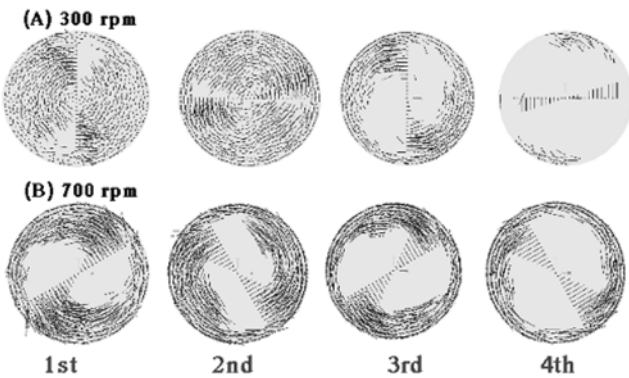

Fig. 10. Velocity pattern of balls at the layer of each stirrer from bottom at rotation speed of stirrer, 300 and 700 rpm.

the position of balls at the wall of pot becomes higher and that at the center of pot becomes deeper.

The movement of balls at the sectional plane of the 2nd stirrer illustrates how the balls move to the wall of the pot with the rotation speed up. That is, as the rotation speed is increased, the balls located near the stirrer move to the pot wall. At 700 rpm, for example, the balls are almost attached to the wall of the pot and form a kind of annular flow pattern of balls. In this case it is thought that the balls have strong centrifugal force and cause such grinding forces as collision, impact, friction, compress and shear to samples.

Fig. 10 shows the velocity patterns of grinding media balls by simulation at the layer of each stirrer from bottom at rotation speed of stirrer, 300 and 700 rpm. The circulating velocity of balls of 300 rpm illustrates that the balls near the stirrer move faster than others. However, the balls of 700 rpm have more average velocity relatively at any position. The circulating velocity of balls is higher than gravitational direction speed in each case. The circulating velocity at 700 rpm is, of course, higher than 300 rpm, but the gravitational direction speed shows not so much difference. That means the balls in the stirrer mill are strongly governed by the rotation speed of the stirrer.

At relatively low rotation speed, the balls are concentrated to the

front side of the stirrer to the direction of rotation, and a few balls are at the back side of the stirrer. However, when the rotation speed is increased, the balls move to the back side of the stirrer because the speed of balls is increased enough to move to the wall of the pot by centrifugal force. That is a different move pattern from one of a tumbling mill [7] which has a critical rotation speed of stirrer and is the reason why the grinding performance depends on the stress intensity, meaning of the kinetic energy of grinding media [1].

2. Contact Forces and Power

Fig. 11 shows a typical profile of power calculated by simulation at 700 rpm, and Fig. 12 shows normal force distributions acting on the stirrers at the rotation speed of stirrer, 300 rpm and 700 rpm. As shown in Fig. 11, at the near starting time the power shows relatively high due to inertia of initial stationary balls caused by the sudden moving of stirrer.

Fig. 13 compares the calculated power by simulation and the experimentally measured power for the rotation speeds of stirrer. The slopes of fitted lines between power and rotation speed of stirrer are changed at 300 rpm. This fact is considered to be related with that the flow pattern of balls is changed with from horizontal flow
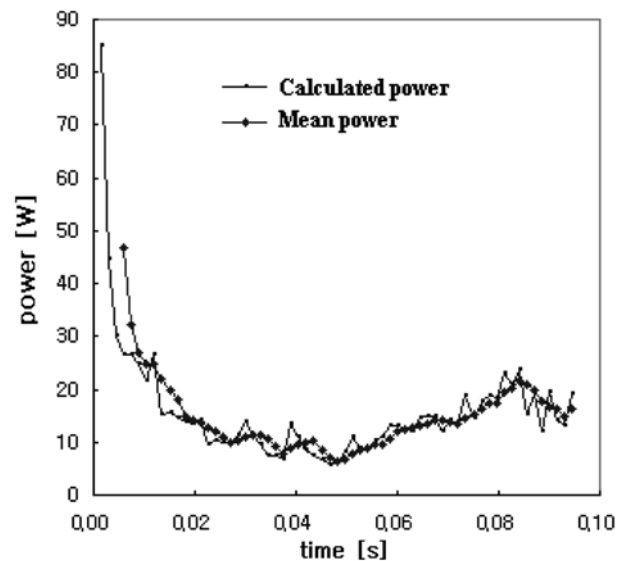

Fig. 11. A typical example of power calculated at 700 rpm.
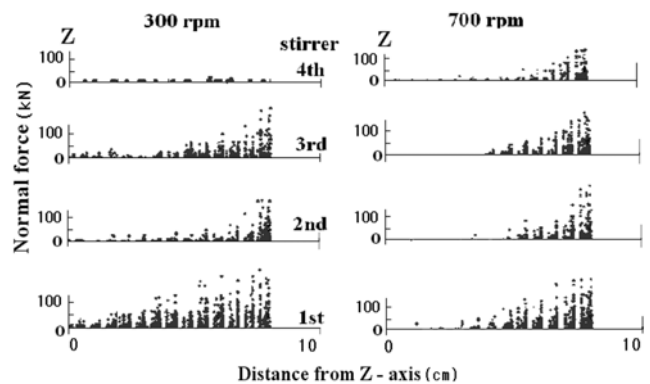

Fig. 12. Normal force distributions acting on the stirrers at rotation speed of stirrer, 300 rpm and 700 rpm.
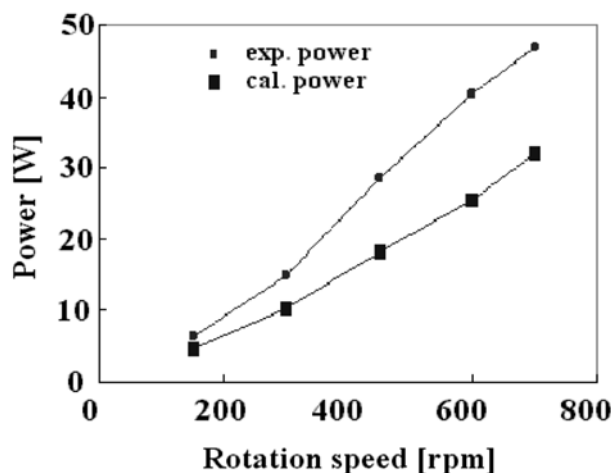
Fig. 13. Comparison of the mean of calculated power and measured one for rotation speed.

Fig. 14. Normal and shear forces distributions of grinding media balls by simulation at rotation speed of stirrer, (a) 300 rpm and (b) 700 rpm.

pattern to annular flow pattern as shown in Fig. 7. There are some gaps between the calculated powers and measured powers due to increase in the loss of energy transfer with rotation speed of stirrer [17].

Fig. 14 shows the typical normal contact force distribution and the shear contact force distribution of grinding media balls by simulation at rotation speed of stirrer, 300 rpm and 700 rpm. The contact forces are increased with increase of rotation speed of stirrer and their variation is considered to have an intimate relationship with grinding characteristics of a stirred media mill.

The contact forces are also increased as the rotation speed of stirrer is increased. The average ratio of shear force and normal force as shown in Table 2 also shows the same tendency. That the ratio of shear force to normal force at 900 rpm (about 34%) is higher than that (about 9%) at 300 rpm is well explained with the behavior of the balls.

The number of contact points is also increased as the rotation speed is increased. As the contact point is the place on which the size reduction occurs actually, the large numbers of contact points means higher probability of the size reduction and can be a necessary condition for the fine grinding because a stirred ball mill is considered to have such important conditions for fine grinding [8].

When the shear forces act on the surface of a particle, it has a kind of grinding mechanism of abrasion, which results from the application of local low intensity surface stress, and the abrasion means the fine grinding mechanism which could be gained by the shear forces as higher rotation speed of the stirred mill. The large normal force acts as fracture that results from the rapid application of intense stress, impact and leads to fragments that are relatively small with respect to the initial particles and having a relatively wide par-
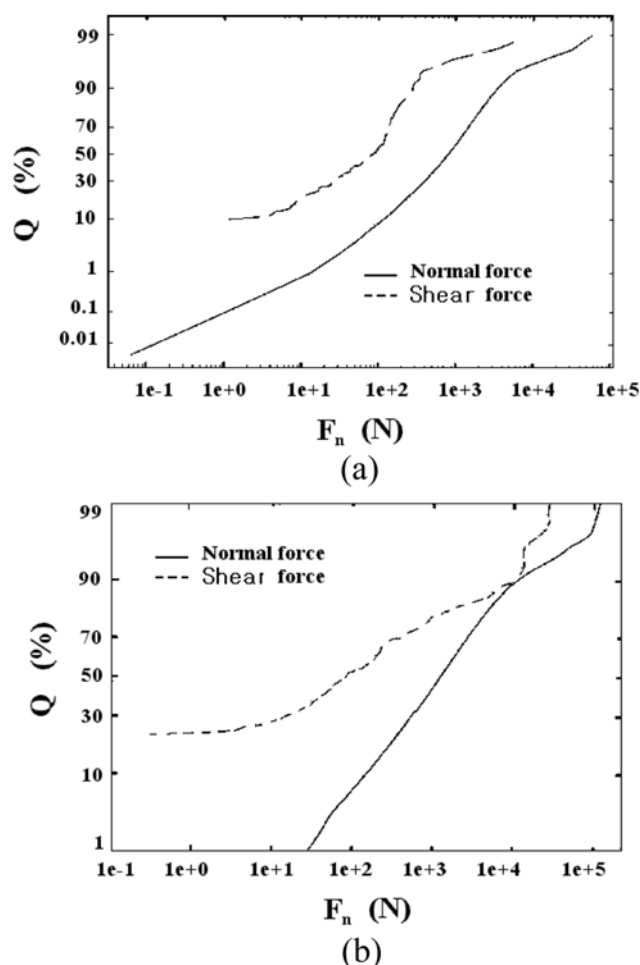
ticle-size distribution. These flow patterns are found to have some relations with contact forces and contact numbers between balls, which affect the grinding behaviors.

CONCLUSION

In a series of grinding processes, a simulation of the motion of grinding media balls in a stirred media mill has been compared with experimental results based on the DEM simulation. The following results are summarized:

(1) DEM is useful for the analysis of ball motion behavior and for grinding mechanism in a stirred mill.

(2) The movement patterns of balls show three types according to the rotation speed of the stirrer.

Table 2. Contact forces and numbers of contact points

Rotation speed (rpm)	Average contact force (g cm/s^2)		Ratio of Fs/Fn	Total no. of contacts point	Average no. of contacts point per ball
	Normal force Fn	Shear force Fs			
300	3,058	283	0.09	27,900	1.61
900	7,474	2,511	0.34	56,000	3.35

· n≤200 rpm: horizontal flow

· n=300 rpm: lower and more vacant at center, higher on the wall of pot

· n≥450 rpm: annular type flow along on the wall of pot

(3) The number of contact points per ball and the shear forces are increased as the rotation speed of stirred is increased.

(4) The calculated and measured power showed the same tendency of variation with the rotation speed of stirrer.

ACKNOWLEDGMENT

REFERENCES

1. A. Kwade, L. Blecher and J. Schwedes, *Powder Technology*, **86**, 59 (1996).
2. W. S. Choi, *J. Soc. Powder Technol.*, *Japan*, **33**, 747 (1996).
3. W. S. Choi, The proceedings of 3rd World Congress on Particle Technology, Brighton (1998).
4. P. A. Cundall and O. D. L. Strack, *Geotechnique*, **29**, 1 (1979).
5. S. Yuu and T. Umekage, *Iron and Steel*, **81**, 11 (1995).
6. P. Radziszewski, *Minerals Engineering*, **12**, 1501 (1999).
7. S. Agrawala, R. K. Rajamani, P. Songfack and B. K. Mishra, *Minerals Engineering*, **2**, 215 (1997).
8. P. W. Cleary, *Mineral Engineering*, **11**, 1061 (1998).
9. A. Datta, B. K. Mishra and R. K. Rajamani, *Canadian Metallurgical Quarterly*, **38**, 133 (1999).
10. P. W. Cleary and D. Hoyer, *Int. J. Miner. Process*, **59**, 131 (2000).
11. M. Gao and E. Forssberg, *Powder Technol.*, **84**, 101 (1995).
12. J. Kano, M. Miyazaki and F. Saito, *Advanced Powder Technology*, **11**, 333 (2000).
13. S. S. Kim and W. S. Choi, *Proceedings of 1st Asian Symposium on Powder Science and Technology*, Bangkok (2000).
14. S. S. Kim and W. S. Choi, *Proceedings of the 43rd Symposium on Powder Science and Technology*, Busan (2005).
15. The Society of Powder Technology, Japan, *Introduction of Powder Simulation*, Sangyodoshyo, Osaka (1998).
16. H. S. Kim and W. S. Choi, *Proceedings of the 8th APCChE Congress*, Seoul (1999).
17. D. W. Fuerstenau and A. Z. M. Abouzeid, *Int. J. Miner. Process*, **67**, 161 (2002).